Contents lists available at ScienceDirect

Journal of Molecular Structure

journal homepage: http://ees.elsevier.com

In silico assessment and sonochemical synthesis of 2-alkynyl 3-chloropyrazines as prospective ligands for SARS-CoV-2

M.V. Satyanarayana [a], Alugubelli Gopi Reddy [b], M. Yedukondalu [c], Mandava Bhuvan Tej [d], Kazi Amirul Hossain [e], Mandava Venkata Basaveswara Rao [f,*], Manojit Pal [g,*]

[a] *Department of Chemistry, Koneru Lakshmaiah Education Foundation, Green fields, Vaddeswaram, Guntur, Andhra Pradesh, India*
[b] *Department of Pharmaceutical Chemistry, Sana college of Pharmacy, Kodad, Telangana, India*
[c] *Department of Chemistry, JNTUA, Ananthapur, Andhra Pradesh, India*
[d] *Department of Pharmacy, Sri Ramachandra Medical College and Research Institute, Porur, Chennai, 600116, India*
[e] *Department of Physical Chemistry, Gdansk University of Technology, Gdańsk, Poland.*
[f] *Department of Chemistry, Krishna University, Machilipatnam-521001, Andhra Pradesh, India.*
[g] *Dr. Reddy's Institute of Life Sciences, University of Hyderabad Campus, Hyderabad 500046, India.*

ARTICLE INFO

Article history:
Received 13 August 2020
Received in revised form 13 January 2021
Accepted 18 January 2021
Available online xxx

Keywords
Chloropyrazine
Alkyne
Ultrasound
In silico study
COVID-19

ABSTRACT

The recent global pandemic caused by COVID-19 has triggered an intense effort worldwide towards the development of an effective cure for this disease. In our effort we have explored the 2-alkynyl substituted 3-chloropyrazine framework as a potential template for the design of molecules for this purpose. Our strategy was supported by the *in silico* studies of representative compounds to assess their binding affinities *via* docking into the N-terminal RNA-binding domain (NTD) of N-protein of SARS-CoV-2. Thus we created a small library of molecules based on the aforementioned template *via* an environmentally safer method that involved the rapid synthesis of 2-alkynyl 3-chloropyrazine derivatives under Cu-catalysis assisted by ultrasound. The reactions proceeded *via* the coupling of 2,3-dichloropyrazine with commercially available terminal alkynes in the presence of CuI, PPh_3 and K_2CO_3 in PEG-400. Further molecular modelling studies helped in establishing a virtual SAR (Structure Activity Relationship) within the series and identification of three potential hits. The desirable ADME was also predicted for these three molecules suggesting their prospective medicinal value.

Introduction

Since the beginning of global pandemic COVID-19 (coronavirus disease 2019) [1], the world health and economy has received a severe blow caused by the novel SARS-CoV-2. An astounding number of people have died in several countries so far [2] and the number of cases of new infections are increasing exponentially every day. The lack of effective vaccines and therapeutic drugs has complicated the situation and allowed spreading of the SARS-CoV-2 worldwide. In view of this urgent need in addressing the ongoing global health problem efforts have been devoted *via* employing diverse approaches to identify effective therapeutics to fight against SARS-CoV-2. In one of these approaches an immunomodulant as well as anti-malaria drug chloroquine (**A**, Fig. 1) has been examined and the *in vitro* studies suggested that the drug might be effective in reducing viral replication in other infections, including the SARS-associated coronavirus (CoV) and MERS-CoV [3,4].

Another drug hydroxychloroquine (a close analogue of **A**) is also being explored as an experimental treatment for COVID-19 [5]. Recently, the drug Favipiravir or T-705 (**B**, Fig. 1) is being explored for this purpose in Japan, India etc. Chemically, Favipiravir is a pyrazine based anti-influenza drug that causes selective inhibition of RNA-dependent RNA polymerase of influenza virus [6]. The other agents that are currently in clinical trials for SARS-CoV-2 mostly include the protease inhibitors e.g. Indinavir, Saquinavir, Darunavir, ASC09, Ritonavir and Lopinavir [7].

The use of nucleocapsid (N)-RNA binding domain as a target protein for the virtual screening of molecules towards finding the potential hit molecules against human coronavirus (CoV-OC43) was explored by Chang *et al* [8]. This protein plays a key role in the packing of viral RNA within the viral envelope into a ribonucleoprotein (RNP) complex (called the capsid), a major part of viral self-assembly and replication. Nevertheless, the quinoline derivative (**C**, Fig. 1) was identified as the most promising compound that was subsequently verified by the experimental results based on surface plasmon resonance (SPR) analysis. The

* Corresponding author.
E-mail addresses: vbrmandava@yahoo.com (M.V.B. Rao); manojitpal@rediffmail.com (M. Pal)

https://doi.org/10.1016/j.molstruc.2021.129981
0022-2860/

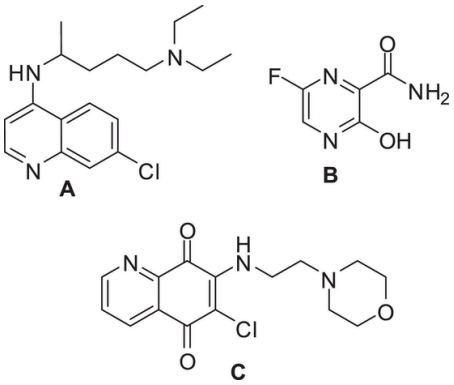

Fig. 1. Example of drugs that are being explored against coronavirus.

crystallographic structure of molecule **C** bound with HCoV-OC43 was deposited. Recently, a crystallographic structure of Apo-Nucleocapsid (RNA-binding domain) of SARS-CoV-2/COVID-19 (PDB: 6M3M) has revealed the potential drug targeting sites [9]. However, efforts towards identification of small organic molecule based inhibitor against Nucleocapsid (N) of SARS-CoV-2 is rather uncommon.

As part of our ongoing research on identification of new and potential agents for COVID-19 we decided to assess the potential of *N*-heterocycle based library of small molecules for this purpose. Consequently, compounds based on the template **D** (Fig. 2) attracted our attention at the initial stage due to the following reasons: (i) the chloro group and pyrazine ring was common in experimental drugs **A** and **B** (Fig. 1) and (ii) the alkyne substituent has been a well-studied moiety in antiviral research [10, 11].

Nevertheless, to validate our predictive rational for picking the template **D** the related docking studies were carried out *in silico*. Firstly, we compared the N-protein of SARS-CoV-2 with HCoV-OC43 both sequentially and structurally to realize the common areas between them. While a 52 % sequence identity was noted in the conserved region based on sequence alignment (see suppl data) our main goal was to search for the secondary structure (to reveal the structural pattern) common in them. Therefore, we performed the secondary structure based sequence alignment (see suppl data) using PRALINE web-tool [12] and pursued the structural comparison in PyMol [13] (Fig. 3). The RMSD was noted as 0.9 Å only whereas the active site residues appeared as conserved. While these data clearly recognized the binding site of SARS-CoV-2 nucleocapsid protein however we carried out the computational binding site prediction by using fconv program [14] for further validation where the same binding cavity was noted with the volume of 279.31 $Å^3$.

To evaluate the binding affinity of few selected molecules, e.g. **3c, 3a** and **3h** (related to the template **D** but possess diversity in the "R" group) along with **C** and **B** against N protein of SARS-CoV-2, we conducted molecular docking study at the nucleotide binding (active) site. While structurally the template **D** was closer to **B** however our main focus was comparing the docking results of compounds based on **D** with **C** rather than **B** because **C** has been reported to be the active molecule for the target pursued in the current study. The protein (PDB: 6M3M) and test molecules were prepared (e.g. energy optimization, charge calculation and addition of hydrogen etc.) using AutoDock tool [15] and all molecules were docked using reliable open-source tool AutoDock Vina [16]. The binding energy of best pose of each molecule is presented in Table 1. Notably, the hydrophobicity and electrostatic surface representation was generated using UCSF Chimera [17] (Fig. 4) for further understanding of the polarity and coulombic electrostatic potential of the binding site (see the following figures). While a balance between hydrophilic and hydrophobic residues was evident in case of N-protein and the binding site was somewhat hydrophobic in nature however it's positive charge was essential for nucleotide binding.

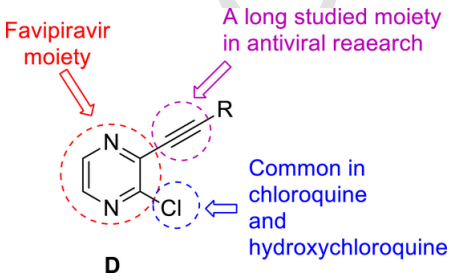

Fig. 2. The 2-alkynyl substituted 3-chloropyrazine as a potential template to target COVID-19

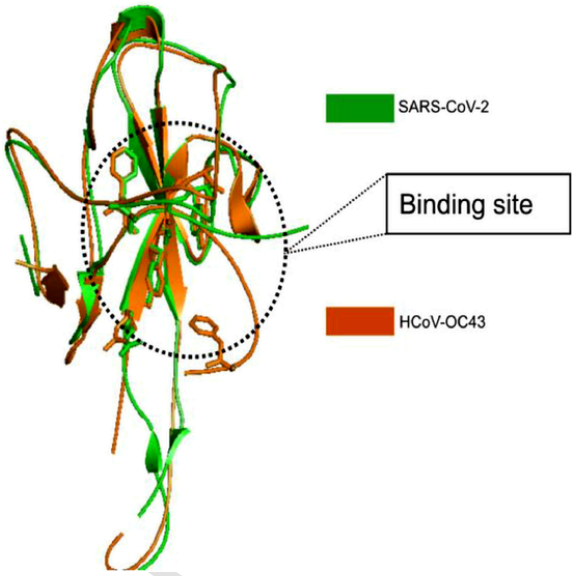

Fig. 3. Structural alignment between RNA-binding domain of nucleocapsid protein of SARS-CoV-2 and HCoV-OC43. Active site residues are shown in stick representation.

It was evident from Table 1 that the binding energy of test molecules especially **3a** was nearly comparable with the known inhibitor **C** (and better than **B**). This clearly suggested that compounds based on framework **D** might interact with the nucleocapsid (N) of SARS-CoV-2 too. Indeed, the molecule **3c** showed (i) a pi-pi interaction with TYR110 and (ii) hydrophobic or VdW contacts with hydrophobic region of polar residue/charged THR55, SER52, ARG150 etc. and with hydrophobic residues like TYR112, ALA51 etc (Fig. 5A). The role of cyclic side chain of **3c** in the close contacts mainly with residues THR55, ALA56, ALA51, TYR110 etc is depicted in the mesh representation (Fig. 5B, see also Fig S-3 in suppl data file). Notably compound **C** showed hydrophobic contacts mainly with residues ALA157, ARG150, THR55, ALA56, ARG89, TYR110 etc (for interaction diagram see Fig S-2 in suppl data file). However, the most effective interactions were observed in case of molecule **3a** as evident from its binding energy (Table 1). The interaction diagram (Fig. 6, see also Fig S-4 in suppl data file) indicated that pyrazine ring of **3a** was involved in a pi-pi interaction with the residue TYR110, and a pi-cation interaction with ARG150. Notably, both TYR110 and ARG150 are important residues in the active site as per the crystallographic data of HCoV-OC43. Nevertheless, **3a** also participated in the hydrophobic/VdW interactions with residues ALA51, SER52, ALA91, ARG89, TYR112, PRO152 etc. and the surface representation showed the closeness of contacts towards those residues.

Table 1
Docking of molecules into N-terminal RNA-binding domain (NTD) of N-protein of SARS-CoV-2. [a]

Molecules	AutoDock Vina score (Kcal/mol)
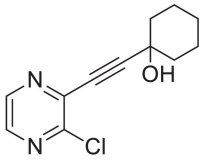 **3c**	-4.9
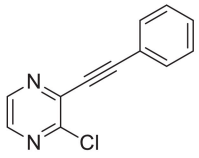 **3a**	-5.0
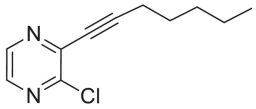 **3h**	-4.4
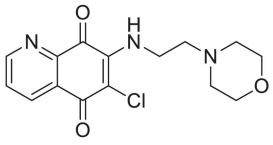 **C**	-5.6
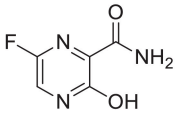 **B**	-4.4

[a] Docking of each individual molecule was performed for 5 times and maximum difference in score was found to be ±0.2.

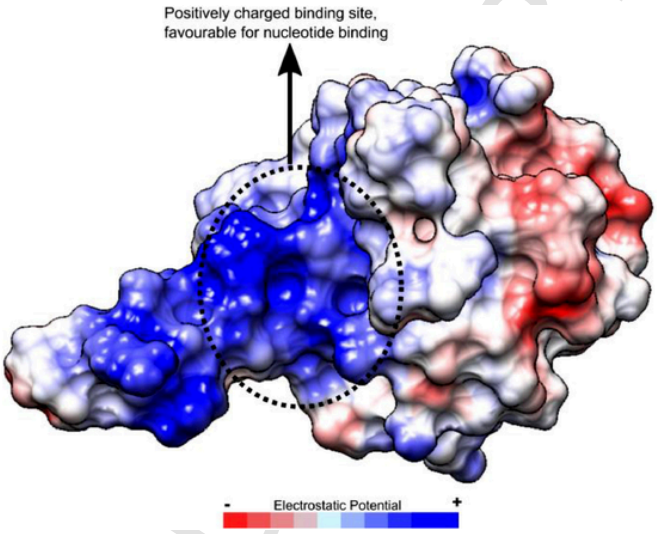

Fig. 4. Electrostatic surface representation of N-protein of SARS-CoV-2

Results and discussion

The synthesis of alkynyl substituted pyrazine or related derivatives have been carried out via the C-C bond forming reaction under the conditions of Sonogashira type coupling [18-22]. Previously, we have also reported the synthesis of 2-alkynyl substituted 3-chloropyrazine *via* a selective mono alkynylation of 2,3-dichloropyrazine (**1**) [23, 24]. The combination of 10%Pd/C-CuI-PPh_3 as a catalyst system, Et_3N as a base and EtOH as a solvent was employed in these reactions. The duration of these reactions was 2-4 h. Nevertheless, all these methodologies involved the use of either a Pd catalyst alone or a combination of Pd and Cu salts. Furthermore, in some of these cases the reactions were performed in organic solvents (e.g. DMF, MeCN, THF etc) that are not environmentally friendly. Because of all these reasons we became interested in exploring a more convenient and environmentally safer method for the synthesis of compounds based on **D** (Fig. 2) including **3a, 3c** and **3h** (Table 1). Thus the synthesis of 2-alkynyl substituted 3-chloropyrazine derivatives (**3**) were undertaken *via* a ultrasound assisted Cu-catalyzed coupling of 2,3-dichloropyrazine (**1**) with commercially available terminal alkynes (**2**) (Scheme 1). The methodology involved the use of PEG-400 as a solvent under mild reaction conditions and does not require the use of any co-catalyst. The details of this study are presented.

The ultrasound irradiation being a useful alternative to the conventional energy sources such as heat, light, or ionizing radiation has

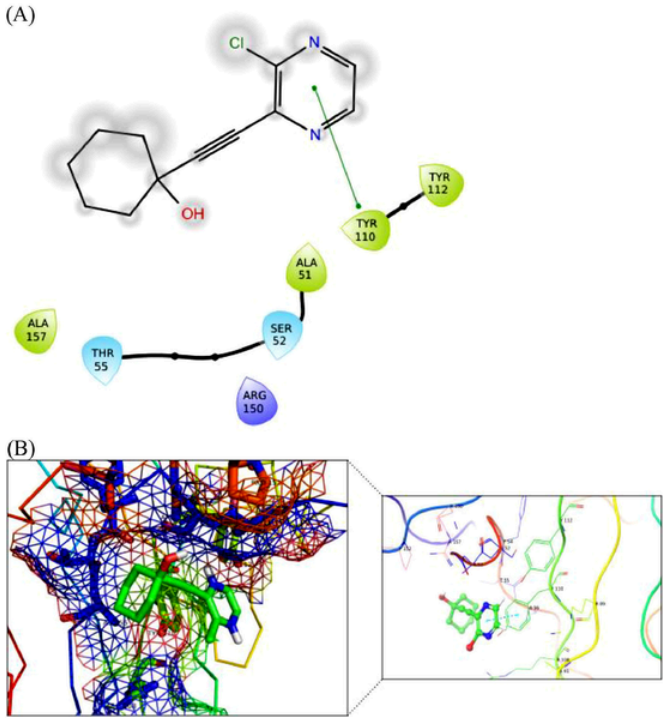

Fig. 5. (A) 2D interaction diagram between compound 3c and N-protein of SARS-CoV-2. (B) Mesh representation of N-protein followed by 3D interaction diagram.

found wide applications in organic synthesis. Indeed, the ultrasound-assisted reactions have become popular approaches particularly in the area of green and sustainable chemistry [25]. The key aspects of these approaches include (i) their environmentally friendly nature (via minimization of waste generation) [26], (ii) decreased energy requirements [27] and (iii) increased efficiency and effectiveness. Indeed, these techniques allow access of target compounds via employing shorter reaction time and milder conditions at the same time increasing the product yields [28, 29]. Being a high boiling, non-hazardous and polar solvent the PEG-400 on the other hand has found applications in various chemical transformations. Indeed, it is considered as one of the environmentally friendly solvents because of its easy recovery from the reaction mixture and recyclability [30]. Thus the combination of ultrasound (as an alternative source of energy) and PEG-400 (as a greener solvent) appeared as an attractive strategy in organic synthesis and hence we became interested in adopting this approach in our current effort. It is worthy to note that while the Sonogashira coupling of iodoarene with terminal alkynes catalyzed by CuI/PPh_3 (i) in PEG-water under microwave heating or reflux in oil bath [31] (at 120 °C) or (ii) in water [32] (at 120 °C) or (iii) under biphasic conditions [33] (water / organic substrates) have been reported earlier, a similar coupling of chloropyrazine with terminal alkynes under ultrasound is not common.

In order to find the optimized reaction conditions for the coupling of 2,3-dichloropyrazine (**1**) with phenyl acetylene (**2a**) was examined under a range of reaction conditions and the results are summarized in Table 2. The reaction proceeded well when carried out using 5 mol% CuI as a catalyst, 30 mol% PPh_3 as a ligand and K_2CO_3 as a base in PEG-400 under ultrasound using a laboratory ultrasonic bath SONOREX SUPER RK 510H model producing irradiation of 35 kHz (entry 1, Table 2). However, the desired coupled product **3a** was obtained in low yield after 8h. The increase of CuI loading to 10 and then 15 mol% improved the product yield to 49 and 75%, respectively (entry 2 and 3, Table 2). Indeed, the reaction was completed within 1h in case of entry 3. This result encouraged us to continue our study for possibility of further improvement in product yield. Hence the catalyst quan-

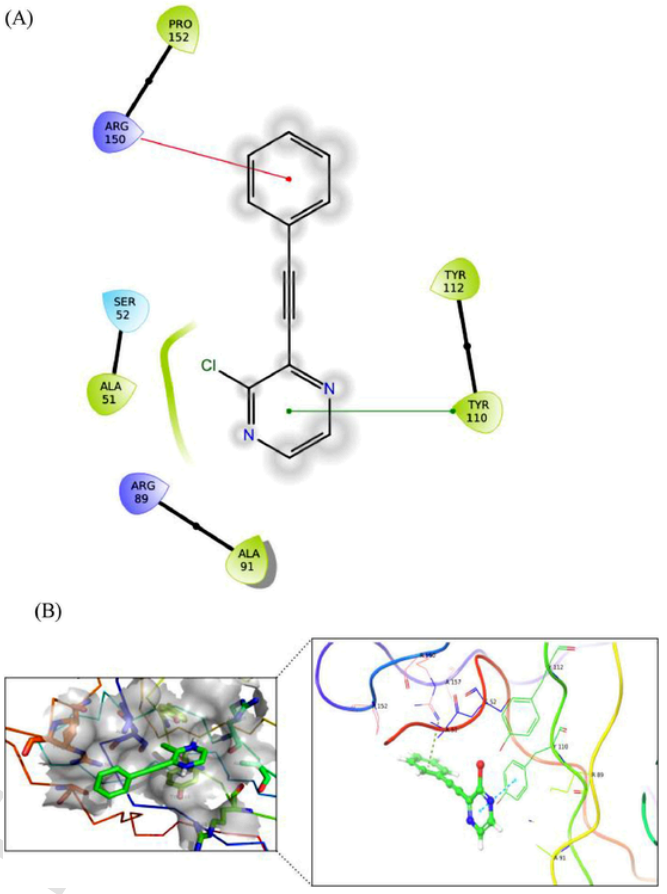

Fig. 6. (A) 2D interaction diagram between N-terminal RNA-binding domain (NTD) of N-protein of SARS-CoV-2 and compound 3a (where pi-pi and pi-cation interaction shown in green and red line respectively), prepared in in Maestro visualizer (Schrödinger, LLC). (B) Surface representation along with 3D interaction diagram (where pi-pi and pi-cation interaction shown in cyan and green dashed line respectively).

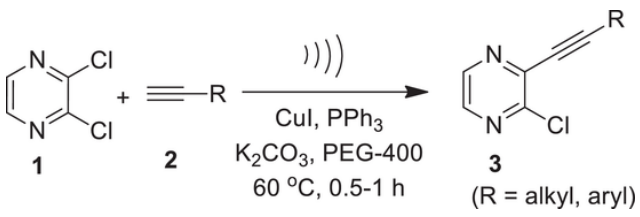

Scheme 1. Cu-catalyzed synthesis of 3-alkynyl substituted 2-chloropyrazines (3) under ultrasound irradiation

tity was increased further from 15 mol% to 20 mol% but no significant increase in yield of **3a** was observed (entry 4, Table 2). The use of other solvent e.g. EtOH or n-BuOH (entry 5 and 6, Table 2) in place of PEG-400 or other base e.g. Et_3N (entry 7, Table 2) in place of K_2CO_3 did not improve the product yield. The use of pure water as a solvent was not successful as the partial hydrolysis of **1** was observed under the conditions employed. We also examined the use of other Cu-catalysts e.g. CuBr or CuCl in the present coupling reaction but these were found to be less effective (entry 8 and 9, Table 2). Notably, the C-C coupling did not proceed in the absence of a catalyst (entry 10, Table 2) indicating key role played by the Cu-sat in the current alkynylation method. Moreover, though the reaction proceeded in the absence of ligand PPh_3 the product yield was not particularly high (entry 11, Table 2). The reaction was also found to be less efficient in terms of product yield when carried out in the absence of ultrasound (entry 12, Table 2). While the reaction temperature was maintained at 50 °C during all reactions as

Table 2
Effect of reaction conditions on coupling of 2,3-dichloropyrazine (**1**) with terminal alkyne (**2a**) [a]

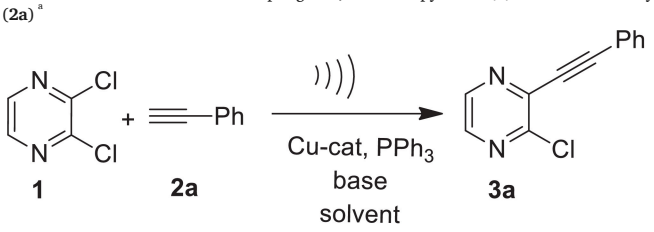

Entry	Cu-cat (mol%)	Base	Solvent	Time (h)	Yield [b]
1.	CuI (5)	K_2CO_3	PEG-400	8	17
2.	CuI (10)	K_2CO_3	PEG-400	4	49
3.	CuI (15)	K_2CO_3	PEG-400	1	71
4.	CuI (20)	K_2CO_3	PEG-400	1	73
5.	CuI (15)	K_2CO_3	EtOH	1	65
6.	CuI (15)	K_2CO_3	n-BuOH	1	64
7.	CuI (15)	Et_3N	PEG-400	4	58
8.	CuBr (15)	K_2CO_3	PEG-400	4	43
9.	CuCl (15)	K_2CO_3	PEG-400	4	30
10.	No catalyst	K_2CO_3	PEG-400	4	No reaction
11.	CuI (15)	K_2CO_3	PEG-400	1	59 [c]
12.	CuI (15)	K_2CO_3	PEG-400	4	47 [d]

[a] All reactions were carried out using the chloro compound **1** (1 equiv.), alkyne **2a** (1 equiv.), a Cu-catalyst, PPh_3 (30 mol%) and base (2 equiv.) in a solvent (5.0 mL) at 50 °C under ultrasound irradiation.
[b] Isolated yields.
[c] The reaction was performed in absence of PPh_3
[d] The reaction was performed in the absence of ultrasound.

mentioned above the decrease and increase of temperature was examined. The reaction did not proceed at lower temperature e.g. at 40 °C and no improvement in product yield was observed at higher temperature e.g. at 70 °C though the reaction progressed well at this temperature. Overall, the condition of entry 3 of Table 2 (i.e. the combination of CuI, PPh_3 and K_2CO_3 in PEG-400 at 50 °C under ultrasound) appeared to be optimum and was used for the preparation of analogues of **3a**.

A range of terminal alkynes (**2**) were employed to couple with the chloro compound (**1**) under the optimized conditions. The alkyne may contain a primary, secondary or tertiary hydroxyl group or an aliphatic chain such as n-propyl, n-butyl, n-pentyl, n-hexyl etc or an aryl group. The Cu-catalyzed C-C bond forming reaction proceeded smoothly in all these cases affording the desired coupled product in good to acceptable yield (Table 3). Notably, a high yield of product was not observed in any of these cases because of the partial dimerization of the terminal alkyne used. The dimerization of terminal alkynes to the corresponding diyne is often known to be a side reaction under the Sonogashira coupling conditions and Cu-salts play a key role in such oxidative homocoupling (Glaser coupling) of terminal alkynes [34-36]. Furthermore, the formation of *bis*-alkynylated product in some cases especially in case of **3c, 3e, 3j** etc (though in trace quantity) perhaps decreased the yield of desired monoalkynylated product. Though the use of reactant alkyne (**2**) was restricted to 1 equivalent to avoid the formation of unwanted *bis*-alkynylated product however the formation of side product could not be suppressed completely. Because of the low boiling point (i.e. 37-38 °C) of 3,3-dimethylbut-1-yne a gradual evaporation of this alkyne was observed under the reaction conditions employed and hence the use of higher quantity of alkyne (1.5 equiv.) was necessary during the preparation of **3b**. The partial hydrolysis of chloro compound **1** was also observed in some cases thereby affecting the product yield. Nevertheless, all the 2-alkynyl substituted 3-chloropyrazine derivatives (**3**) synthesized were characterized via the spectral (^{1}H and

Table 3
Synthesis of 3-alkynyl substituted 2-chloropyrazine derivatives (**3**) [a, b] (Scheme 1).

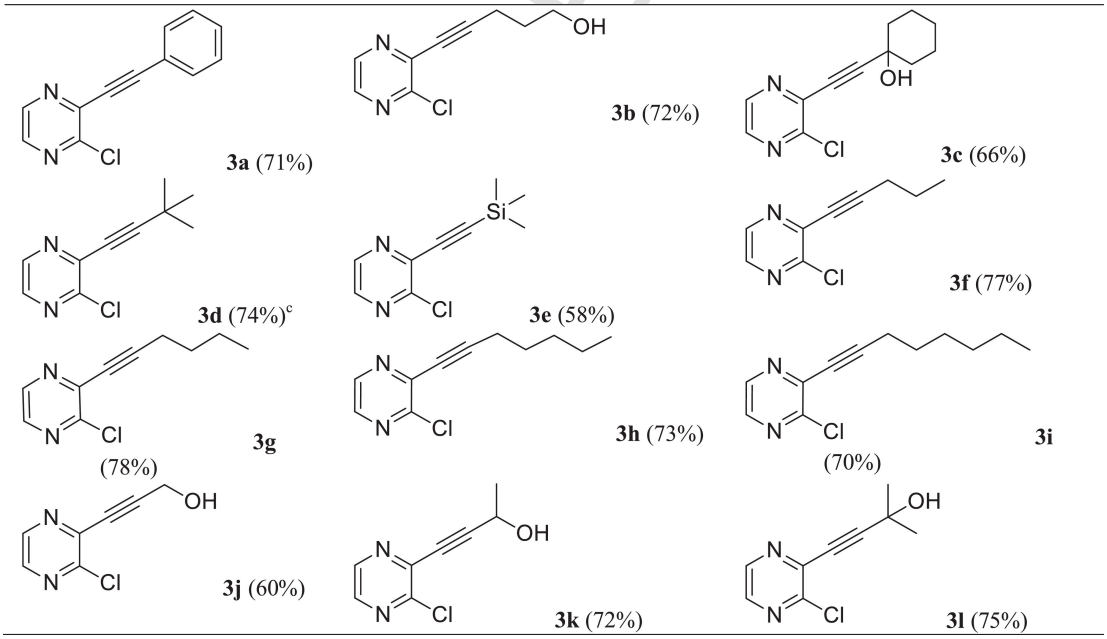

[c]1.5 equivalent of alkyne (3,3-dimethylbut-1-yne) was used in this case.
[a] All reactions were carried out using the chloro compound **1** (1 equiv.), alkyne **2** (1 equiv.), CuI (15 mol%), PPh_3 (30 mol%) and K_2CO_3 (2 equiv.) in PEG-400 (5.0 mL) at 50 °C under ultrasound irradiation for 0.5-1h.
[b] Figure in the bracket represents isolated yield.

^{13}C NMR and Mass) data. The partial ^{1}H and ^{13}C NMR data of a representative compound **3d** is presented in Fig. 7. It is evident that the methyl protons of *t*-butyl group appeared at 1.37 δ in the ^{1}H NMR spectra whereas the C-5 and C-6 protons of the pyrazine ring appeared at 8.24 and 8.43 δ. The methyl carbons of *t*-butyl group appeared at 30.3 ppm in the ^{13}C NMR spectra whereas the carbon bearing all these Me groups appeared at 28.4 ppm. The ^{13}C NMR signals at 75.5 and 108.8 ppm were due to the two sp-hybridized carbons of alkyne moiety and the signal at 150.7 ppm was due to the aromatic carbon bearing the chloro group. The presence of alkyne moiety was further supported by the IR absorption near 2240 cm^{-1}.

In the light of results of Table 2 and previous reports [31-33] a proposed Cu-catalytic cycle depicting the coupling of **1** with **2** under ultrasound irradiation is presented in Scheme 2. The interaction of CuI with PPh_3 under ultrasound irradiation afforded the Cu(I) complex (**A**) that was the actual catalytic species to catalyze the C-C coupling. The complex **A** then interacted with the terminal alkyne (**2**) in the presence of K_2CO_3 to give the intermediate **E-1** and KI. Next, the interaction of **E-1** with the chloro compound (**1**) produced a copper cluster (**E-2**) linked with both alkyne as well as heteroarene moiety. The **E-2** then in the presence of ligand and ultrasound afforded the desired product **3** and the Cu-species **E-3.** On interaction with KI the **E-3** regenerated the

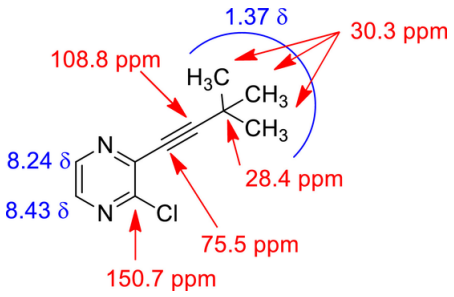

Fig. 7. Partial representation of ^{1}H and ^{13}C NMR spectral data of compound 3d.

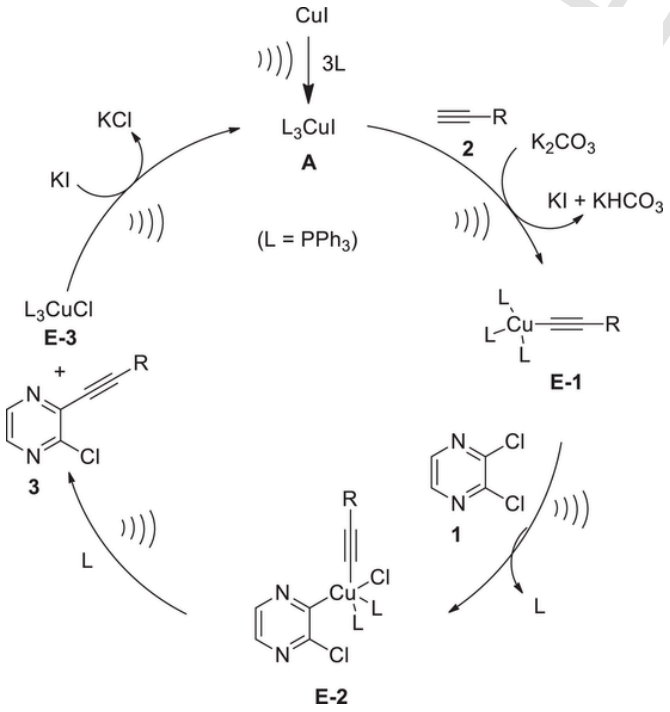

Scheme 2. The proposed Cu-catalytic cycle for the ultrasound assisted coupling of 1 with 2

catalyst **A** to complete the catalytic cycle. It was evident from the results of Table 2 that the C-C coupling was accelerated significantly by the ultrasound irradiation. This may be explained as follows: ultrasound generally causes the compression of the liquid and then rarefaction (expansion) resulting in a sudden pressure drop that forms small oscillating bubbles of gaseous substances. These bubbles with each cycle of the applied ultrasonic energy continue to expand till they reach to an unstable size. Then the collision and /or violent collapse of these cavitation bubbles raise the local temperature within the reaction medium. This promotes [37] the facile crossing of energy barrier thereby faster conversion of reactants to intermediates and subsequently to product(s) within a short reaction time. The acceleration of various steps of Scheme 2 by ultrasound in this way explains the rapid formation of product **3** from the reactants **1** and **2**.

Having synthesized a library of molecules (**3**) based on **D** (Fig. 2) we re-focused on assessing their binding affinities via docking into the N-terminal RNA-binding domain (NTD) of N-protein of SARS-CoV-2 (PDB: 6M3M). The purpose of this study was to gain some insights regarding the virtual SAR (Structure-Activity-Relationship) within this series of compounds. The results are presented in Table 4 including that of

Table 1 for head-to-head comparison and discussion. It was evident that most of the compounds showed good to or moderate binding affinities (> 4.0 Kcal/mol) except the compound **3e** (for which the docking study was not performed). The nature and size of the substituent (other than the chloropyrazine moiety) attached to the alkyne moiety appeared to have played a key role in binding affinities (> 4.0 Kcal/mol) except the compound **3e** (for which the docking study was not performed). The nature and size of the substituent (other than the chloropyrazine moiety) attached to the alkyne moiety appeared to have played a key role in binding with the protein *in silico* (Fig. 8). For example, the *in silico* study of less active compound **3g** (Fig. 9) indicated the absence of pi-pi interaction with TYR110. Moreover, the butyl side chain in this case was not favorable in adopting the proper orientation. Indeed, due to the hindrance caused by the ARG150, PRO152 and ALA51 at the top site and limited flexibility of the butyl side chain, the molecule **3g** could not adopt any other suitable orientation. In other words, the molecular volume of ALA51, PRO152, and ARG150 (shown as spheres in Fig S-5, suppl data file) was responsible for the probable clashes with the butyl side chain. On the other hand, the compound **3i**

Table 4
Docking of molecules into N-terminal RNA-binding domain (NTD) of N-protein of SARS-CoV-2. [a]

Compound	AutoDock Vina score (Kcal/mol)
3a	-5.0
3b	-4.5
3c	-4.9
3d	-4.5
3e	n.d.
3f	-4.2
3g	-4.1
3h	-4.4
3i	-4.8
3j	-4.2
3k	-4.3
3l [b]	-4.5
Compound **C** [b]	-5.6
Compound **B** [b]	-4.3

n.d. = not done
[a] See the footnote of Table 1.
[b] Reference compound (see Table 1).

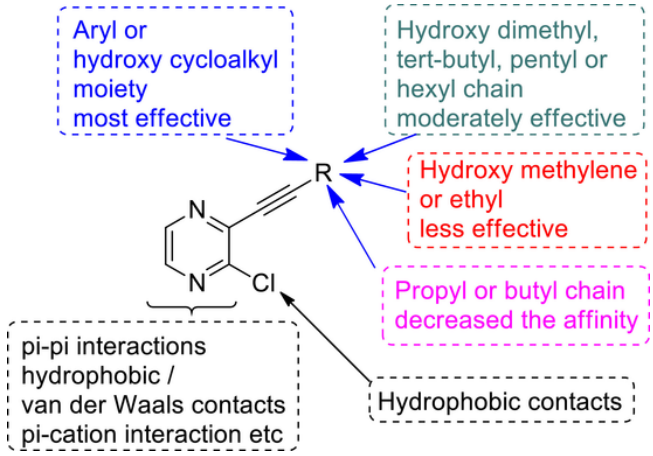

Fig. 8. Summary of *in silico* binding affinities of compound 3

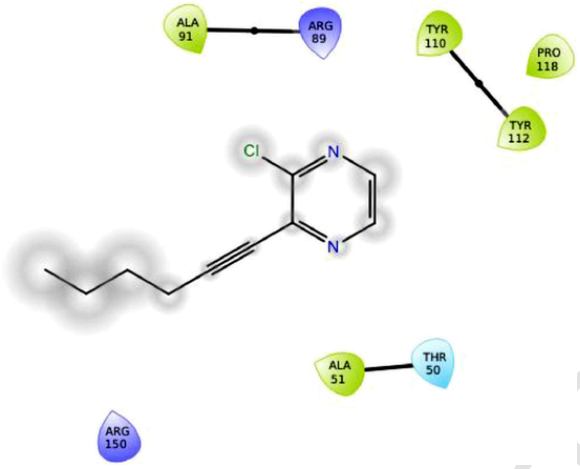

Fig. 9. The 2D interaction diagram of compound 3g with N-protein of SARS-CoV-2.

though possesses a longer side chain (n-hexyl moiety) showed relatively better binding affinity. Indeed, because of its higher flexibility (e.g. total number of rotatable bond 6 vs 4 of compound **3g**) the molecule could adopt a favorable orientation at the active site and able to stack on TYR110 that allowed its participation in a pi-pi interaction (Fig. 10). Moreover, the steric hindrance caused by ALA51 and ARG150 was avoided in this case due to the folding of alkyl chain to a different direction (see Fig S-6, suppl data file). The molecule participated in hydrophobic interactions with residues ALA51, ALA56, PHE54, SER52, THR55, ARG89, etc. It is worthy to mention that while the pyrazine ring was involved in the pi-pi interaction in most of the cases the chloro group was prominently involved in hydrophobic contacts mainly with residues that were in close proximity. Notably, while the pi-interactions were missed in case of reference compound **C** its participation in a number of effective hydrophobic contacts was reflected by its good binding affinity. Nevertheless, though none of the synthesized pyrazine derivatives (**3a-l**) showed better binding affinities than **C** however several of them were found to be better than Favipiravir (compound **B**) in terms of binding affinities (Table 4). Indeed, Favipiravir showed fewer interactions (e.g. a H-bond with the backbone atom of GLY117 at distance of 2.43Å and some van der Waals / hydrophobic interaction with residues THR50, ALA51, TYR112, THR149, and PRO118) when docked into the N-protein of SARS-CoV-2 (see Fig S-7, suppl data). Nevertheless, the compound **3a, 3c** and **3i** appeared as potential agents for further studies.

Next, to gain some initial assessment about ADME (absorption, distribution, metabolism, and excretion) or pharmacokinetic properties of

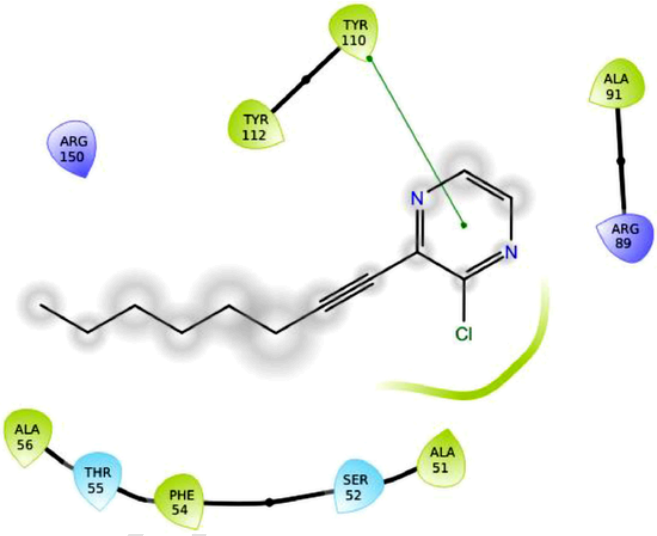

Fig. 10. 2D interaction diagram of compound 3i and N-protein of SARS-CoV-2.

3a, 3c and **3i** *in silico* the computational ADME prediction of these compounds was carried out using SwissADME web-tool [38] (Table 5, among the various descriptors only notable one are listed in the table). Indeed, this study predicted the desirable ADME for all three compounds except **3c**. The reason for predicting **3c** to be a substrate of P-gp was perhaps the presence of hydroxycycloalkyl moiety. Nevertheless, besides their high GI absorption no violation of Lipinski or Veber rule was noted for all these compounds that showed the bioavailability score 0.55. Overall, the compound **3a** emerged as a potential hit molecule for further evaluation towards the identification of prospective agent against COVID-19. Currently, assessing the effect of **3a** on the RNA-binding affinity of nucleocapsid proteins by surface plasmon resonance (SPR) experiment is being planned.

Conclusions

In conclusion, we have explored the 2-alkynyl substituted 3-chloropyrazine framework as a potential template for the design of molecules targeting COVID-19. Initially the *in silico* evaluation was carried out using few representative molecules *via* assessing their binding affinities against the N-terminal RNA-binding domain (NTD) of N-pro-

Table 5
Computational ADME prediction of **3a, 3c** and **3i**

Properties	Molecules		
(i) Physicochemical	**3a**	**3c**	**3i**
Molecular Weight (g/mol)	214.65	236.70	222.71
Consensus Log P [a]	2.65	2.15	3.40
Log S (ESOL) [b] (soluble)	-3.53 (soluble)	-2.78 (soluble)	-3.86
(ii) Pharmacokinetics			
GI [c] absorption	High	High	High
P-gp [d] substrate	No	Yes	No
Lipinski rule	No violation	No violation	No violation
Veber rule	No violation	No violation	No violation
Bioavailability score	0.55	0.55	0.55

[a] Log P: Lipophilicity.
[b] Log S (ESOL): water solubility, calculated by ESOL method which is a Quantitative Structure-Property Relationship (QSPR) based model.
[c] GI: Gastrointestinal.
[d] P-gp: permeability glycoprotein.

tein of SARS-CoV-2. The promising results of this study triggered further assessment of these molecules. Consequently, efforts were devoted to build a library of molecules based on the designed framework. Thus, the target molecules were synthesized via a Cu-catalyzed C-C bond forming reaction under ultrasound irradiation. This rapid and environmentally safer method allowed a convenient access to the 2-alkynyl substituted 3-chloropyrazine derivatives via the coupling of 2,3-dichloropyrazine with commercially available terminal alkynes in the presence of CuI, PPh_3 and K_2CO_3 in PEG-400. The methodology was free from the use of bi-metallic salts as catalysts and furnished the desired products in acceptable yields. Further *in silico* studies of these compounds helped in establishing a virtual SAR (Structure Activity Relationship) within the series and identification of three potential hit molecules. The desirable ADME was also predicted for these three molecules. Overall, besides describing a Cu-catalyzed ultrasound assisted rapid and greener approach towards the synthesis of 2-alkynyl 3-chloropyrazine derivatives the current study also unveiled a prospective framework for the design and discovery of new agents targeting COVID-19.

Credit author statement

M. V. Satyanarayana, Alugubelli Gopi Reddy, M. Yedukondalu and Mandava Bhuvan Tej were involved in the preparation, isolation, purification and characterization of all the target compounds presented in the current manuscript.

Kazi Amirul Hossain was involved in performing all the *in silico* studies.

Mandava Venkata Basaveswara Rao and Manojit Pal were responsible conceptualization, coordination and overall supervision of the entire work presented in the submitted manuscript.

Supplementary data

Supplementary data associated with this article can be found, in the on line version, at xxxxxxxxx

Declaration of Competing Interest

The authors declare that they have no known competing financial interests or personal relationships that could have appeared to influence the work reported in this paper.

Acknowledgement

The authors thank the management of Dr. Reddy's Institute of Life Sciences, Hyderabad, India, for continuous support and encouragement.

Supplementary materials

Supplementary material associated with this article can be found, in the online version, at doi:10.1016/j.molstruc.2021.129981.

References

[1] P. Zhou, X.L. Yang, X.G. Wang, B. Hu, L. Zhang, W. Zhang, H.–R. Si, Y. Zhu, B. Li, C.-L. Huang, H.–D. Chen, J. Chen, Y. Luo, H. Guo, R.–D. Jiang, M.–Q. Liu, Y. Chen, X.–R. Shen, X. Wang, X.–S. Zheng, K. Zhao, Q.–J. Chen, F. Deng, L.–L. Liu, B. Yan, F.X. Zhan, Y.–Y. Wang, G.–F. Xiao, Z.–L. Shi, A pneumonia outbreak associated with a new coronavirus of probable bat origin, Nature. 579 (2020) 270–273, doi:10.1038/s41586-020-2012-7.

[2] Coronavirus (COVID-19); World Health Organization; https://who.sprinklr.com/, accessed on May 7, 2020.

[3] A. Savarino, J.R. Boelaert, A. Cassone, G. Majori, R. Cauda, Effects of chloroquine on viral infections: an old drug against today's diseases?, Lancet Infect. Dis. 3 (2003) 722–727.

[4] P. Colson, J.–M. Rolain, D. Raoult, Chloroquine for the 2019 novel coronavirus SARS-CoV-2, Int. J. Antimicrob. Agents 55 (2020) 105923.

[5] A. Cortegiani, G. Ingoglia, M. Ippolito, A. Giarratano, S. Einav, A systematic review on the efficacy and safety of chloroquine for the treatment of COVID-19, J. Critical Care. (2020) in press, doi:10.1016/j.jcrc.2020.03.005.

[6] Y. Furuta, B.B. Gowen, K. Takahashi, K. Shiraki, D.F. Smee, D.L. Barnard, Favipiravir (T-705), a novel viral RNA polymerase inhibitor, Antivir. Res. 1002 (2013) 446–454.

[7] C. Harrison, Coronavirus puts drug repurposing on the fast track, Nature Biotechnol 38 (2020) 379–381.

[8] C.K. Chang, S. Jeyachandran, N.J. Hu, C.L. Liu, S.Y. Lin, Y.S. Wang, Y.–M. Chang, M.H. Hou, Structure-based virtual screening and experimental validation of the discovery of inhibitors targeted towards the human coronavirus nucleocapsid protein, Molecular BioSystems 12 (2016) 59–66.

[9] S. Chen, S. Kang, 6M3M: Structural insights of SARS-CoV-2 nucleocapsid protein RNA binding domain reveal potential unique drug targeting sites. RSCB PDB; doi:10.2210/pdb6m3m/pdb.

[10] E. De Clercq, M. Cools, J. Balzarini, R. Snoeck, G. Andrei, M. Hosoya, S. Shigeta, T. Ueda, N. Minakawa, A. Matsuda, Antiviral activities of 5-ethynyl-1-beta-D-ribofuranosylimidazole-4-carboxamide and related compounds, Antimicrob. Agents Chemother. 35 (1991) 679–684, doi:10.1128/aac.35.4.679.

[11] Y.F. Shealy, C.A. O'Dell, G. Arnett, W.M. Shannon, Synthesis and antiviral activity of the carbocyclic analogs of 5-ethyl-2′-deoxyuridine and of 5-ethynyl-2′-deoxyuridine, J. Med. Chem. 29 (1986) 79–84, doi:10.1021/jm00151a013.

[12] V.A. Simossis, J. Heringa, PRALINE: a multiple sequence alignment toolbox that integrates homology-extended and secondary structure information, Nucleic Acids Res 33 (Issue suppl_2) (2005) W289–W294, doi:10.1093/nar/gki390.

[13] W.L. DeLano, Pymol: An open-source molecular graphics tool, CCP4 Newsletter On Protein Crystallography 40 (2002) 82–92.

[14] G. Neudert, G. Klebe, fconv: format conversion, manipulation and feature computation of molecular data, Bioinformatics 27 (2011) 1021–1022, doi:10.1093/bioinformatics/btr055.

[15] G.M. Morris, R. Huey, W. Lindstrom, M.F. Sanner, R.K. Belew, D.S. Goodsell, A.J. Olson, Autodock4 and AutoDockTools4: automated docking with selective receptor flexiblity, J. Comput. Chem. 16 (2009) 2785–2791.

[16] O. Trott, A.J. Olson, AutoDock Vina: improving the speed and accuracy of docking with a new scoring function, efficient optimization, and multithreading, J. Comput. Chem. 31 (2010) 455–461, doi:10.1002/jcc.21334.

[17] E.F. Pettersen, T.D. Goddard, C.C. Huang, G.S. Couch, D.M. Greenblatt, E.C. Meng, T.E. Ferrin, UCSF Chimera - A Visualization System for Exploratory Research and Analysis, J. Comput. Chem. 25 (2004) 1605–1612.

[18] C. Schindler, C. Schulzke, Pyrazine- and pyridine-substituted prop-2-yn-1-ols, but-3-yn-2-ols, and but-3-yn-2-ones – purification, stability, and handling revised, Chem. Heterocycl. Compd. 51 (2015) 1008 Khim. Geterotsikl. Soedin. 2015, 51, 1008.

[19] P. Meti, E.-S. Lee, J.-W. Yang, Y.-D. Gong, Regioselective synthesis of dipyrrolopyrazine (DPP) derivatives via metal free and metal catalyzed amination and investigation of their optical and thermal properties, RSC Adv 7 (2017) 18120–18131.

[20] M. Zubair, A.C. Ghosh, C. Schulzke, The unexpected and facile molybdenum mediated formation of tri- and tetracyclic pentathiepins from pyrazine-alkynes and sulfur, Chem. Commun. 49 (2013) 4343–4345.

[21] A.D. Sonawane, A. Shimozuma, T. Udagawa, M. Ninomiyaa, M. Koketsu, Synthesis and photophysical properties of selenopheno [2,3-b]quinoxaline and selenopheno [2,3-b]pyrazine heteroacenes, Org. Biomol. Chem. 18 (2020) 4063–4070.

[22] V.P. Mehta, S.G. Modha, D. Ermolat'ev, K.V. Hecke, L.V. Meervelt, E.V. Van der Eycken, Diversity-Oriented Synthesis of Substituted Furo [2,3-b]pyrazines, Australian J. Chem. 62 (2009) 27–41, doi:10.1071/CH08376.

[23] A. Nakhi, M.S. Rahman, G.P.K. Seerapu, R.K. Banote, K.L. Kumar, P. Kulkarni, D. Haldar, M. Pal, Transition metal free hydrolysis/cyclization strategy in a single pot: synthesis of fused furo N-heterocycles of pharmacological interest, Org. Biomol. Chem. 11 (2013) 4930–4934.

[24] S.K. Kolli, A. Nakhi, R. Medishetti, S. Yellanki, P. Kulkarni, R.R. Raju, M. Pal, NaSH in the construction of thiophene ring fused with N-heterocycles: A rapid and inexpensive synthesis of novel small molecules as potential inducers of apoptosis, Bioorg. Med. Chem. Lett. 24 (2014) 4460–4465.

[25] T.J. Mason, Ultrasound in synthetic organic chemistry, Chem. Soc. Rev. 26 (1997) 443–451.

[26] R. Cella, H. A. Stefani, Ultrasonic Reactions, in Green Techniques for Organic Synthesis and Medicinal Chemistry (eds W. Zhang and B. W. Cue), John Wiley & Sons, Ltd, Chichester, UK. doi: 10.1002/9780470711828.ch13, 2012.

[27] L. Pizzuti, M.S.F. Franco, A.F.C. Flores, F.H. Quina, C.M.P. Pereira, Recent Advances in the Ultrasound-Assisted Synthesis of Azoles, in: M. Kidwai, N.K. Mishra (Eds.), Green Chem. - Environ. Benign Approaches, IntechOpen, 2012, doi:10.5772/35171.

[28] B.Kaur S. Puri, H.Kumar A. Parmar, Applications of Ultrasound in Organic Synthesis - A Green Approach, Curr. Org. Chem. 17 (2013) 1790–1828.

[29] D.N.K. Reddy, K.B. Chandrasekhar, Y.S. Siva Ganesh, G.R. Reddy, J.P. Kumar, R.K. Kapavarapu, M. Pal, FeF_3-catalyzed MCR in PEG-400: ultrasound assisted synthesis of N-substituted 2-aminopyridines, RSC Adv 6 (2016) 67212–67217, doi:10.1039/c6ra14228a.

[30] J. Chen, S.K. Spear, J.G. Huddleston, R.D. Rogers, Polyethylene glycol and solutions of polyethylene glycol as green reaction media, Green Chem 7 (2005) 64–82.

[31] G. Chen, J. Xie, J. Weng, X. Zhu, Z. Zheng, J. Cai, Y. Wan, CuI/PPh3/PEG–Water: An Efficient Catalytic System for Cross-Coupling Reaction of Aryl Iodides and Alkynes, Synth. Commun. 41 (2011) 3123–3133, doi:10.1080/00397911.2010.517363.

[32] J.T. Guan, G.-A. Yu, L. Chen, T.Q. Weng, J.J. Yuan, S.H. Liu, CuI/PPh_3-catalyzed Sonogashira coupling reaction of aryl iodides with terminal alkynes in water in the absence of palladium, Appl. Organometal. Chem. 23 (2009) 75–77, doi:10.1002/aoc.1474.
[33] Y. Liu, V. Blanchard, G. Danoun, Z. Zhang, A. Tlili, W. Zhang, F. Monnier, A.V.D. Lee, J. Mao, M. Taillefer, Copper-Catalyzed Sonogashira Reaction in Water, Chem. Select 2 (2017) 11599–11602, doi:10.1002/slct.201702854.
[34] N. Krause, S. Thorand, Improved Procedures for the Palladium-Catalyzed Coupling of Terminal Alkynes with Aryl Bromides (Sonogashira Coupling), J. Org. Chem. 63 (1998) 8551–8553.
[35] S.B. Rosenblum, T. Huynh, A. Afonso, H.R. Davis, Synthesis of 3-Arylpropenyl, 3-Arylpropynyl and 3-Arylpropyl 2-Azetidinones as Cholesterol Absorption Inhibitors: Application of the Palladium-Catalyzed Arylation of Alkenes and Alkynes, Tetrahedron 56 (2000) 5735–5742.
[36] M.A. Brimble, G.S. Pavia, R.J. Stevenson, A facile synthesis of aryldihydropyrans using a Sonogashira–selenoetherification strategy, Tetrahedron Lett 43 (2002) 1735–1738.
[37] K.S. Suslick, D.A. Hammerton, R.E. Cline, Sonochemical hot spot, J. Am. Chem. Soc. 108 (1986) 5641–5642.
[38] A. Daina, O. Michielin, V. Zoete, SwissADME: a free web tool to evaluate pharmacokinetics, drug-likeness and medicinal chemistry friendliness of small molecules, Sci. Rep. 7 (2017) 1–13.